Analytical Study of Low-Field Diffusive Transport in Highly Asymmetric Bilayer Graphene Nanoribbon

Sitangshu Bhattacharya and Santanu Mahapatra, *Member, IEEE*

***Abstract*—We present a simplified theory of carrier backscattering coefficient in a twofold degenerate asymmetric bilayer graphene nanoribbon (BGN) under the application of a low static electric field. We show that for a highly asymmetric BGN ($\triangle = \gamma$), the density of states in the lower subband increases more that of the upper, in which $\triangle$ and γ are the gap and the interlayer coupling constant, respectively. We also demonstrate that under the acoustic phonon scattering regime, the formation of two distinct sets of energy subbands signatures a quantized transmission coefficient as a function of ribbon width and provides an extremely low carrier reflection coefficient for a better Landauer conductance even at room temperature. The well-known result for the ballistic condition has been obtained as a special case of the present analysis under certain limiting conditions which forms an indirect validation of our theoretical formalism.**

***Index Terms*—Bilayer graphene, nanoribbon, scattering, transmission.**

I. Introduction

ELECTRONS in a bilayer graphene (BG) move with a Fermi velocity, which is about 300 times less than that of the speed of light. This marks the central importance of the graphene sheet in mesoscopic devices and interconnects [1], [2]. BG is primarily a zero bandgap material, but can be modulated to act as a semiconductor by applying either an external bias [3] or by changing the doping profile in the two coupled hexagonal lattices with an A'–B-type stacking pair [4]. In both cases, this results in a potential difference between the layers, which may be called symmetric or asymmetric, depending on whether the difference is zero or nonzero, respectively [5]. Thus, by varying the bias or the doping concentration, one can modulate the magnitude of the bandgap in graphene-based devices, and this may find interesting applications in low dimensional photonics.

Recently, quantum Hall and cyclotron experiments were carried out in a pure symmetric 2-D graphene sheet [6]–[8] for the realization of extremely high carrier mobility. Theoretical investigations have already been proposed to explain such high mobility [9], [10] within the limitations of acoustic phonon scattering. In an asymmetric 2-D BG, the conduction and valance bands are two-fold degenerate. Since the carriers are confined in a 2-D plane, a further structural confinement along the lateral direction transforms the 2-D system to a 1-D one. Such a system may be called a BG nanoribbon (BGN). The resulting lateral quantum well leads to the generation of discrete energy eigenvalues due to the van Hove singularity (VHS) condition. There has been a recent advancement in probing a few electronic properties of BG within the frame work of tight binding (TB) formalism [11]–[13]. The extensive analyses of Hwang and Das Sarma [9] and Kubakaddi [10] suggest that although BG has an extremely nonlinear band structure, the overlap integral can be avoided since the Coulomb potential does not play a role in the determination of the phonon matrix element. Their arguments fit well in explaining the room-temperature electron mobility in BG, which is about 10^5 $\mathrm{cm^2 \cdot V^{-1} \cdot s^{-1}}$ and can also be experimentally realized [14]. With such high electron mobility and a large mean free path length (MFP) [15], it would be interesting to determine the acoustic-phonon-dominated MFP in a degenerate highly asymmetric BGN for its potential applications in nanoscale device interconnects technology.

In this paper, we present a simplified theoretical formulation of the carrier back-scattering coefficient in a BGN within the framework of TB formalism. Since the diffusive Landauer conductance is directly proportional to the transmission coefficient, we will also investigate how this conductance is affected with the change in lateral and longitudinal lengths and a static longitudinal applied field. The paper is organized as follows. In Section II-A, we will derive the expression of the electron density of states in a BGN using the TB approach. This is followed by the derivation of the longitudinal acoustic (LA) phonon scattering rate in Section II-B. Section II-C deals with the determination of the isotropic carrier back-scattering length and Landauer diffusive conductance within LA phonon-scattering regime and in the presence of a longitudinal static electric field. Finally, in Section III, we present the results and discussion.

II. Theoretical Background

A. Formulation of the Electron Density of States in BGN

For an asymmetric BG sheet, the TB formalism leads to the electron Hamiltonian near the K point as [5], [7]

$$H = \begin{pmatrix} -\triangle/2 & 0 & 0 & \pi^\dagger \\ 0 & \triangle/2 & \pi & 0 \\ 0 & \pi^\dagger & \triangle/2 & \gamma \\ \pi & 0 & \gamma & -\triangle/2 \end{pmatrix} \tag{1}$$

in which $\triangle = \phi_1 - \phi_2$, $\phi_i s$ are the onsite potentials on each monolayer, $\pi\{= v_F \hbar(-i\frac{\partial}{\partial x} + \frac{\partial}{\partial y})\}$ is the Berry phase momentum operator [5], γ is the interlayer coupling constant [5] and

Manuscript received November 11, 2009; revised January 19, 2010; accepted February 5, 2010. Date of publication February 18, 2010; date of current version May 11, 2011. This work was supported by the Department of Science and Technology (DST), India, under Grant SR/FTP/ETA-37/08. The review of this paper was arranged by Associate Editor M. P. Anantram.

The authors are with the Nano-Scale Device Research Laboratory, Centre for Electronics Design and Technology, Indian Institute of Science, Bangalore 560012, India (e-mail: isbsin@yahoo.co.in; santanu@cedt.iisc.ernet.in).

Color versions of one or more of the figures in this paper are available online at http://ieeexplore.ieee.org.

Digital Object Identifier 10.1109/TNANO.2010.2043443

1536-125X/$26.00 © 2010 IEEE

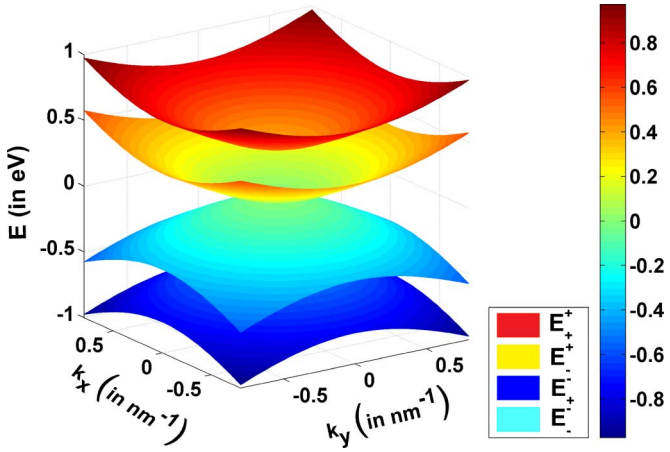

Fig. 1. E–k dispersion surface of an asymmetric BG.

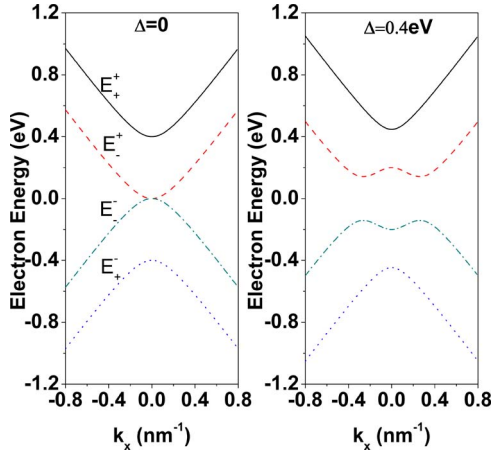

Fig. 2. E–k dispersion curve of symmetric ($\triangle = 0$) and asymmetric ($\triangle \neq 0$) BG.

v_F is the Fermi velocity. Assuming a Bloch-type wave function, the electron dispersion relation can be evaluated as (see the Appendix)

$$\left[k_x^2 + k_y^2 - \left(\frac{E - \triangle/2}{\hbar v_F}\right)^2\right]\left[k_x^2 + k_y^2 - \left(\frac{E + \triangle/2}{\hbar v_F}\right)^2\right] = \gamma^2\left[\frac{E^2 - \triangle^2/4}{(\hbar v_F)^4}\right] \tag{2}$$

in which E is the electron energy as measured from the edge of the conduction band in the vertically upward direction. Equation (2) generates two sets of two degenerate bands, namely, E_+^+, E_-^+, E_-^-, and E_+^-. Fig. 1 exhibits the energy spectrum for an asymmetric BG. The constant energy surfaces are the circles in the k_x–k_y plane. With the increase of asymmetry, the gap opens, as shown in Fig. 2. For an asymmetric BGN, (2) transforms to

$$k_{x_\pm}^{\pm} = \pm\frac{1}{\hbar v_F}\left[E^2 + \frac{\triangle^2}{4} - \left(\frac{n_y \pi \hbar v_F}{l_y}\right)^2 \pm \sqrt{E^2\left(\gamma^2 + \triangle^2\right) - \gamma^2\triangle^2/4}\right]^{1/2} \tag{3}$$

where $n_y (=1, 2, 3, \ldots)$ and l_y are the VHS quantum numbers and the ribbon width along the y-direction, respectively. Fig. 3(a) exhibits the energy subband structure of a 10-nm-wide asymmetric BGN. It appears that with an increase in $\triangle$, there is no intermixing of the lower and upper set of subband levels. For $l_y = 10$ nm, there is a considerable opening of the gap about the zero level. However, as the ribbon width is reduced further, the bulging nature of the lower subband curves near $k_x = 0$ smoothen up. This essentially means that with the increase in $\triangle$, less energy is required to transfer the electrons to the higher subbands near $k_x = 0$. Also, we notice that as we increase $\triangle$, the subband energies for the lower sets decrease. This means that the carriers are more populated in the lower subbands than in the upper, and this creates a population inversion. Hence, for very narrow width BG, it is expected that a negative differential conductance might occur. Using (3) and the spin and valley

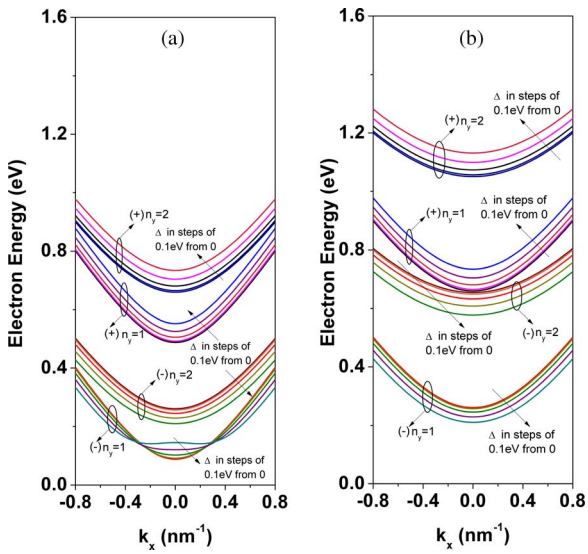

Fig. 3. E–k dispersion curves of (a) 10 nm and (b) 5 nm BGN with varying $\triangle$. With the increase in $\triangle$, energies of the lower subband decrease, while for upper subbands they increase. For 10nm BGN, we see the bulging nature near $k_x = 0$, while no bulging occurs for 5 nm BGN. Thus, as the ribbon thickness is reduced, a population inversion occurs where the lower subbands are more populated than the higher.

degeneracy ($g_s = g_v = 2$) [16], the electron density of states in an asymmetric BGN for both the lower $(-)$ and upper $(+)$ set of energy subbands can be derived as

$$N_{1\text{-D}}^{\pm} = \frac{g_s g_v}{\pi \hbar v_F}\sum_{n_y=1}^{n_{y\max}}\left\{\left[E \pm \frac{E\left(\gamma^2 + \triangle^2\right)/2}{\sqrt{E^2\left(\gamma^2 + \triangle^2\right) - \left(\gamma^2\triangle^2/4\right)}}\right] \times \left[E^2 + \frac{\triangle^2}{4} - \left(\frac{n_y \pi \hbar v_F}{l_y}\right)^2 \pm \sqrt{E^2\left(\gamma^2 + \triangle^2\right) - \frac{\gamma^2\triangle^2}{4}}\right]^{-1/2} H\left(E - E_{n_y}^{\pm}\right)\right\} \tag{4}$$

in which H is the Heaviside step function and the subband energies are given by the condition $k_x^{\pm}=0$, in which E is replaced by $E_{n_y}^{\pm}$, where, $E_{n_y}^{\pm}=(1/2^{1/2})\times[\varsigma(n_y)\pm\sqrt{\varsigma^2(n_y)-4\xi(n_y)}]^{1/2}$, $\varsigma(n_y)=\gamma^2+\frac{\Delta^2}{2}+2((n_y\pi\hbar v_F/l_y))^2$, and $\xi(n_y)=\frac{\Delta^2}{16}+\frac{\gamma^2\Delta^2}{4}-(\Delta^2/2)(n_y\pi\hbar v_F/l_y)^2+(n_y\pi\hbar v_F/l_y)^2$.

However, for a highly asymmetric case ($\triangle=\gamma$), (3) and (4) reduce to

$$k_x^{\pm}=\frac{1}{\hbar v_F}\left[E^2+\frac{\gamma^2}{4}-\left(\frac{n_y\pi\hbar v_F}{l_y}\right)^2\pm\sqrt{2E^2\gamma^2-\frac{\gamma^4}{4}}\right]^{1/2} \tag{5}$$

and

$$N_{1\text{-D}}^{\pm}=\frac{g_s g_v}{\pi\hbar v_F}\sum_{n_y=1}^{n_{y\max}}\left\{\left[E\pm\frac{E\gamma}{\sqrt{2E^2-(\gamma^2/4)}}\right]\times\left[E^2+\frac{\gamma^2}{4}-\left(\frac{n_y\pi\hbar v_F}{l_y}\right)^2\pm\gamma\sqrt{2E^2-\frac{\gamma^2}{4}}\right]^{-1/2}\times H\left(E-E_{n_y}^{\pm}\right)\right\}. \tag{6}$$

B. Formulation of the Acoustic Phonon-Scattering Rate

The momentum relaxation rate using Fermi's Golden rule can be written as [17]

$$\frac{1}{\tau_{k,k'}}=\frac{2\pi}{\hbar}\sum_{k'}\sum_{q}\left\{|M(k,k')|^2(1-\cos\theta)\times\left(N_q+\frac{1}{2}\pm\frac{1}{2}\right)\delta(E-E'\mp\hbar\omega)|I_{fi}|^2\right\} \tag{7}$$

in which $|M(k,k')|$ is the phonon matrix element, N_q is the phonon number governed by Bose–Einstein statistics, δ is the Dirac-delta function, $\omega=v_{\text{ph}}q$, v_{ph} is the phonon velocity, and q and k' are the phonon and the scattered electron wave vector, respectively. $\mp$, in this case, indicates an LA phonon emission and absorption condition and θ is the angle between the incoming and scattered electron wave vector. The quantity $|I_{fi}|^2$, in this case, is defined as the form factor that characterizes the condition whether there would be an interband ($f\neq i$) or intraband ($f=i$) subband carrier transition. Following [9], the phonon matrix for graphene can be written as $|M(k,k')|=(D^2\hbar q/2A\rho v_{\text{ph}})[1-(q/2k)^2]$, where D is the acoustic deformation potential constant in electron volts, $A(=Ll_y)$ is the area of the sample, L is the longitudinal length, and ρ is the material density in kilograms per meter square. It may be noted that a more general approach to the phonon dispersion relation has been carried out recently [18] between the first, second, and third nearest neighbor interactions by imposing the lattice symmetry of graphene. Since, however, in the present case, the phonon velocity is smaller than that of the electron Fermi velocity, without losing any generality, we can assume $q=2k\sin(\theta/2)$ [9], [19]. Using the fact that the LA phonon scattering is elastic and the lateral quantum well is of infinite height, the momentum relaxation rate for both the lower and upper set of subbands assumes the form

$$\frac{1}{\tau_{fi}^{\pm}}=\frac{\pi^2D^2k_BT}{g_sg_v\hbar\rho v_{\text{ph}}^2}\left(\frac{1}{l_{y_{fi}}}\right)N_{1\text{-D}}^{\pm}(E) \tag{8}$$

in which $1/l_{y_{fi}}=(1/l_y)(2+\delta_{fi})$. The Kronecker delta condition $i=f$ gives intraband transition, whereas $i\neq f$ gives interband transition.

C. Formulation of the Carrier Back-Scattering in a BGN

The isotropic carrier back-scattering length can be written as [20]

$$\lambda_{fi}^{\pm}(E)=2v_x(E)\tau_{fi}^{\pm}(E) \tag{9}$$

in which $v_x(E)$ is the carrier subband velocity along the x-direction. Thus, using (3), (4), and (8), the isotropic back-scattering length per subband in both the upper and lower sets in the presence of a drain potential $v_D(x)$ can approximately be written as

$$\lambda_{fi}^{\pm}(E)=\frac{2\hbar^2\rho v_F^2v_{\text{ph}}^2}{\pi D^2k_BT}\left(\frac{l_y}{2+\delta_{fi}}\right)\left(\epsilon\pm\frac{\gamma}{\sqrt{2}}\right)^{-2}\times\left[\epsilon\left(\epsilon\pm\sqrt{2}\gamma\right)+\frac{\gamma^2}{4}-\left(\frac{n_y\pi\hbar v_F}{l_y}\right)^2\right] \tag{10}$$

in which $\epsilon=E+ev_D(x)$. Using (10) and assuming the left and right velocities ($v^{\mp}(x)$) of the carriers ($n^{\mp}(x)$) remains the same ($v^+(x)=v^-(x)=v(x)$) as the boundary condition and $n^-(L)=0$ as the current continuity equation, the equation for the 1-D-directed flux per subband in both the upper and lower sets following McKelvey's method [21] assumes the form

$$n^+(x)v^+(x)=-\left(n^+(0)-n^-(0)\right)\frac{v(0)}{\lambda_{0_{fi}}}\times\int\left[1-f_{\pm}\left(\frac{2\epsilon\pm b}{\epsilon^2\pm b\epsilon+c(n_y)}\right)+e_{\pm}\left(\frac{1}{\epsilon^2\pm b\epsilon+c(n_y)}\right)\right]dx \tag{11}$$

in which $\lambda_{0_{fi}}=(\hbar^2\rho v_F^2v_{\text{ph}}^2/2\pi D^2)(l_y/(2+\delta_{fi}))$, $b=\sqrt{2}\gamma$, $c(n_y)=[\gamma^2/4-(n_y\pi\hbar v_F/l_y)^2]$, $f_{\pm}=(\sqrt{2}/2)[1\mp1]\gamma$, and $e_{\pm}(n_y)=(\gamma^2/4)+(n_y\pi\hbar v_F/l_y)^2\pm\gamma^2[1\mp1]$. Integrating, and rearranging the terms at $x=0$, we get the total reflection coefficient (R_{fi}) for both the upper and lower set of subbands for the present case as

$$R_{fi}=\left.\frac{n^-(0)}{n^+(0)}\right|_{fi}=\left(\frac{1}{N}\right)\left[\frac{R_{+_{fi}}R_{-_{fi}}}{R_{+_{fi}}+R_{-_{fi}}}\right] \tag{12}$$

where N is the total number of subbands, $R_{\pm_{fi}}=\sum_{n_y=1}^{n_{y\max}}[L_{kT}\xi_{\pm}(\epsilon,n_y)/(\lambda_{0_{fi}}+L_{kT}\xi_{\pm}(\epsilon,n_y))]$, $L_{kT}(=k_BT/eE_0)$ is the distance over which the potential drops to the value k_BT/e of its maximum at the source terminal, E_0 is the constant electric field applied along the longitudinal length (between the source

and drain terminal) and

$$\xi_{\pm}(\epsilon, n_y) = eE_0 L - f_{\pm} ln \left| \frac{c(n_y) + \epsilon(\epsilon \pm b)}{c(n_y) + E(E \pm b)} \right| + \left\{ \frac{e_{\pm}(n_y)}{\sqrt{b^2 - 4c(n_y)}} ln \left| \left\{ \frac{(2\epsilon \pm b) - \sqrt{b^2 - 4c(n_y)}}{(2E \pm b) - \sqrt{b^2 - 4c(n_y)}} \right\} \times \left\{ \frac{(2E \pm b) - \sqrt{b^2 - 4c(n_y)}}{(2\epsilon \pm b) - \sqrt{b^2 - 4c(n_y)}} \right\} \right| \right\}. \quad (13)$$

In the limit $E_0 \rightarrow 0$, (12) converges to

$$R_{fi} \rightarrow \frac{1}{2N} \left(\frac{L}{\lambda_{fi} + L} \right) \quad (14)$$

where, $\lambda_{fi} = \lambda_{0_{fi}}/k_B T$.

Since almost all the carriers at the Fermi level take part in the conduction mechanism, the net carrier-degeneracy statistics for carriers at the upper and lower set of subbands can be written as

$$n_{1\text{-D}} = \frac{g_s g_v}{2\pi\hbar v_F} \sum_{n_y=1}^{n_{y\max}} \left[2k_B T \left\{ F_0(\eta) - ln \left(1 + \frac{E_F - ev_D}{\sqrt{2}\gamma} \right) \right\} - \frac{c(n_y)}{\sqrt{2}\gamma} \left\{ \frac{47}{48} - \varrho(E_F - ev_D) \right\} \right] \quad (15)$$

in which $\eta = (1/k_B T)\{E_F - \sqrt{2}\gamma - ev_D\}$, $\varrho(E_F) = (\sqrt{2}\gamma/E_F)[1 - (1/4)(\sqrt{2}\gamma/E_F) + (1/6)(\sqrt{2}\gamma/E_F)^2 + (1/16)(\sqrt{2}\gamma/E_F)^3]$ and $F_j(\eta)$ is the one-parameter Fermi–Dirac integral of order j [22]. Using (12), the diffusive conductance of the carriers at the Fermi level can be written from the Landauer–Buttiker formulation as

$$G_{fi} = \frac{2e^2}{h}(T_{fi}) \quad (16)$$

in which T_{fi} is the transmission coefficient.

III. Results and Discussions

Using $\gamma = 0.4$ eV [4], [23], $D = 19$ eV, $\rho = 7.6 \times 10^{-7}$ kg/m^2, $v_F = 10^6$ m/s, and $v_{\text{ph}} = 2 \times 10^4$ m/s for a graphene sheet [9], [10], we have plotted the scattering rate as a function of the carrier energy in Fig. 4 for $l_y = 10$ nm at 300 K. For both symmetric and asymmetric BGN, the presence of γ and $\triangle$ has a profound effect on the density of states function. For a symmetric system, states are more available in the upper set of subbands rather than in the lower. However, with an increase in the electron energy in a highly asymmetric BGN, by comparing with the corresponding subband energies in the lower and upper sets, we see that the states in the lower set of subbands increase rather than in the upper. This remarkable property of population inversion signatures the use of asymmetric BGN in the area of optical electronics. Since there is a 1-D carrier motion in a BGN, the inclusion of subband energies owing to Born-Von Karman boundary conditions (BVK) leads to a discontinuity in the density-of-states function due to the VHS of the wave vectors. This joint handshaking of both BVK and VHS signatures quantized behavior in many physical and transport properties of BGN. As our formalism is based on the low longitudinal-biased system, we have restricted ourselves to only elastic acoustic phonon scattering for the present system which mainly determines the ribbon conductance [9]. However, for a high biased system, the interaction is mainly determined by inelastic scattering between the electron and optical phonons and (8) no longer holds good.

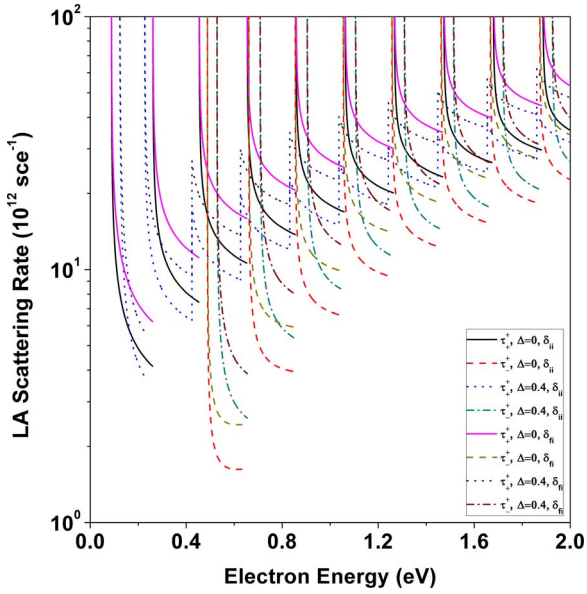

Fig. 4. LA phonon scattereing rate in a symmetric BGN with $l_y = 10$ nm at $T = 300$ K. It appears that with an increase of $\triangle$ and E, states at the lower subband are populated more than in the upper.

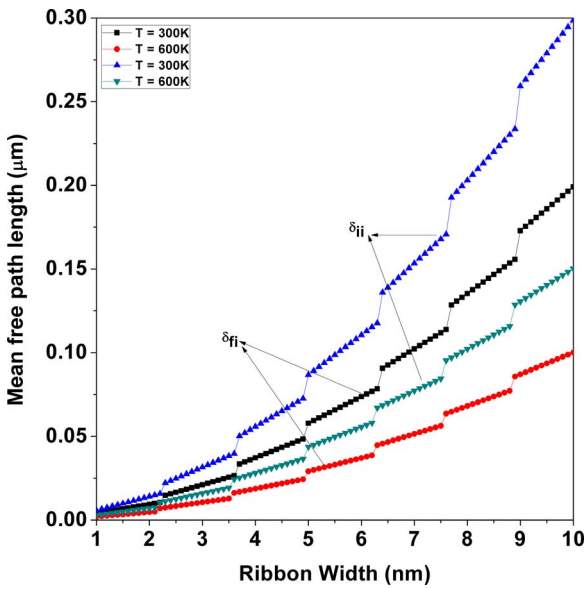

Fig. 5. MFP length as a function of well thickness for a highly asymmetric ($\triangle = \gamma$) BGN for $E_0 = 10^6$ V/m and $n_{1\text{-D}} = 10^9$ m^{-1} at different temperatures.

Using (10) and (15), we have numerically plotted the MFP at different temperatures as a function of ribbon width in Fig. 5 for a highly asymmetric BGN by including both inter- and intra-subband scattering. It appears that the MFP increases with the ribbon width. Since the dispersion relation of an asymmetric

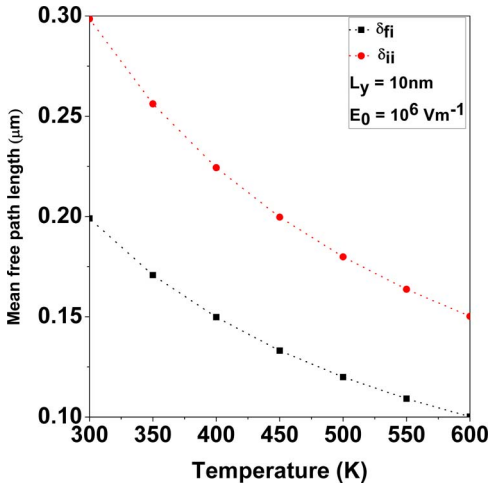

Fig. 6. MFP length as a function of temperature for a highly asymmetric ($\triangle = \gamma$) BGN for $l_y = 10$ nm, $E_0 = 10^6$ V/m and $n_{1\text{-D}} = 10^9$ m^{-1}.

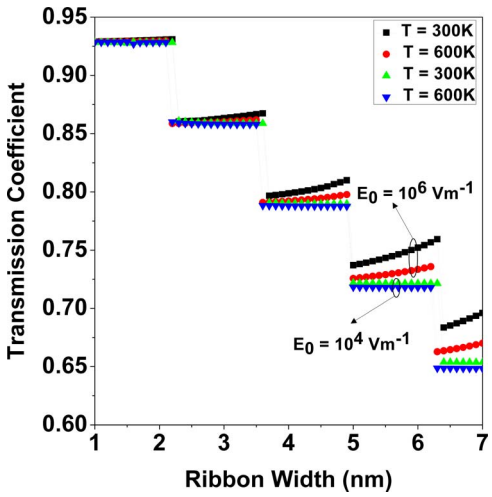

Fig. 7. Intrasubband transmission coefficient as a function of ribbon width for a highly asymmetric ($\triangle = \gamma$) BGN for $E_0 = 10^6$ V/m and $n_{1\text{-D}} = 10^9$ m^{-1} at different temperatures.

BGN is highly nonlinear due to the presence of γ and $\triangle$, the rate of increment of λ between two singularities is not uniform. In general, MFPs are functions of electron energy. However, when the system is nondegenerate, the carrier's energy can be represented mainly due to thermal energy [17]. This is in sharp contrast to materials having high carrier degeneracy, since, in such a case, the carriers' Fermi energy is much larger than that of thermal energy. It is also exhibited from the same figure that even at room temperature, the intrasubband acoustic phonon scattering may lead to an MFP of about 300 nm for a ribbon width of 10 nm (see Fig. 6). It may also be noted that the MFP, in general, depends on the subband energies. The electron energies, in this case, are restricted close to that of the Fermi energy, so that the back scattering of the electrons due to the acoustic phonon can be profoundly achieved. Fig. 7 exhibits the variation of the transmission coefficient for intrasubband scattering as a function of ribbon width for different values of the electric field. It appears that T_{fi} decreases in a step-like manner. At this point,

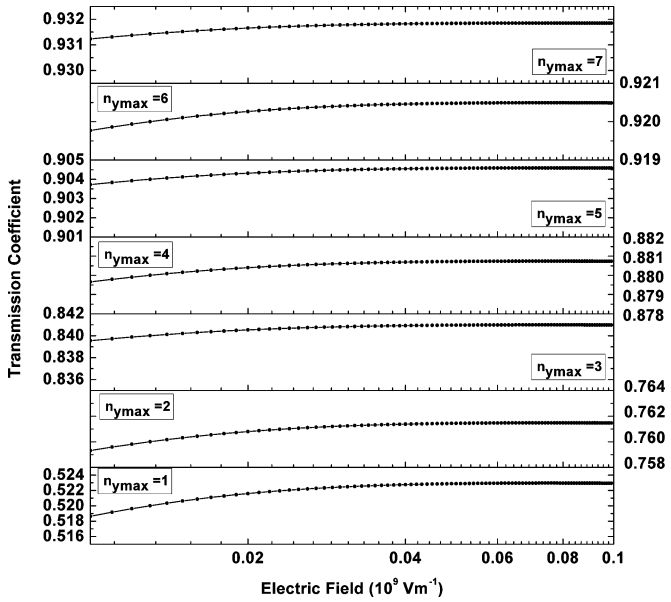

Fig. 8. Intrasubband transmission coefficient as a function of electric field for a highly asymmetric ($\triangle = \gamma$) BGN for $l_y = 1$ nm, $L = 300$ nm, $T = 300$ K, and $n_{1\text{-D}} = 10^9$ m^{-1} for different subbands.

it may be noted that in a high electric field, Fermi energy tends to increase since more carriers are generated. This is the reason why the T_{fi} for a particular subband will increase, although the incorporation of all the subbands due to the increment in lateral dimension will reduce T_{fi}, and hence, the Landauer conductance G_{fi}. Another physical explanation for this decreasing behavior is that since the Fermi energy is reduced with the increase in ribbon width, this reduces the overall G_{fi}. However, with the decrease in the magnitude of the electric field, carriers cease to generate, and thus, T_{fi} becomes nearly constant until a new subband generates. The step dependencies are due to the crossing over of the Fermi level by the size-quantized levels. For each coincidence of a size-quantized level with the Fermi level, there is a discontinuity in the density-of-states function resulting in a quantum jump. The appearance of humps in the curves of Figs. 5 and 7 are due to the redistribution of the electrons among the quantized energy levels when the size quantum number corresponding to the highest occupied level changes from one fixed value to another. From Fig. 7, we see that more than 92% of carriers are transmitted to the drain from the source even at room temperature for a longitudinal length of 300 nm. At this point, we note that for degenerate wires with extremely low lateral dimensions (as in this case), neglecting quantized energies may not provide an in-depth solution. Thus, one also has to take the subband energies for more accurate analysis that significantly alters the scattering coefficient. This fact has been exhibited in Fig. 8 for different subbands. The net effect of including all the subbands for both the sets increases the total T_{fi}.

From (14), we also see that in a low electric field, the contribution to R_{fi} from both the upper and lower sets of subbands is equal to $L/4N\,(\lambda + L)$ and it is independent of the lateral well width, and thus, the subband number. However, this must not be construed to mean that the equal reflection suffered from

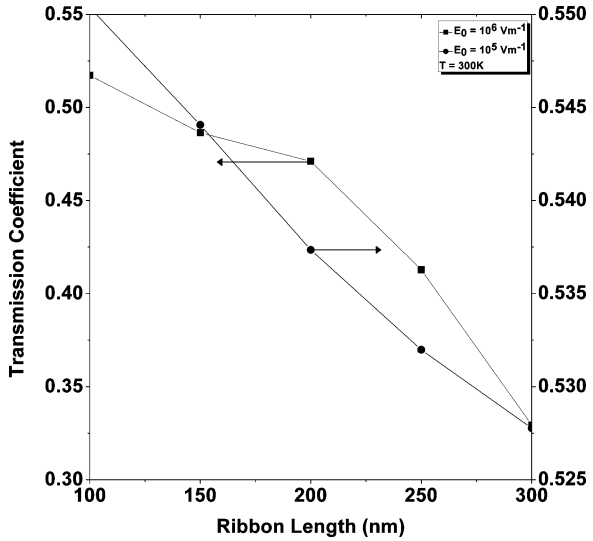

Fig. 9. Intrasubband transmission coefficient as a function of ribbon length for a highly asymmetric ($\triangle = \gamma$) BGN for $l_y = 10$ nm, $T = 300$ K, and $n_{1\text{-D}} = 10^9$ m^{-1} for different electric field.

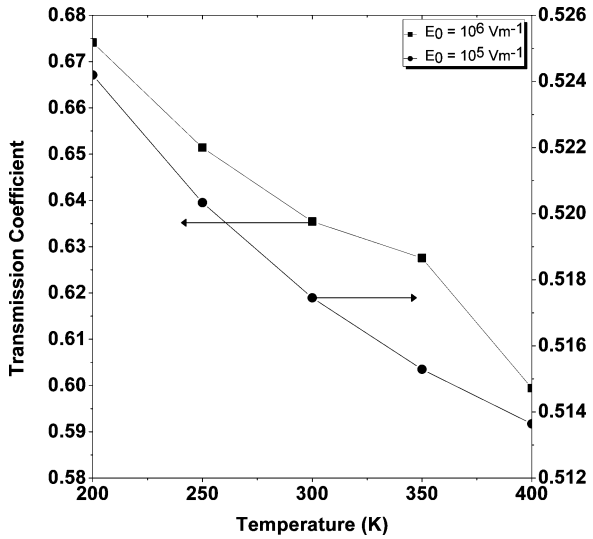

Fig. 10. Intrasubband transmission coefficient as a function of temperature for a highly asymmetric ($\triangle = \gamma$) BGN for $l_y = 5$ nm, $L = 300$ nm, and $n_{1\text{-D}} = 10^9$ m^{-1} for different electric field.

the drain in both sets of subbands means that an equal number of carriers are present. This logic is entirely satisfactory in the sense of the difference in the density of states in each band [see (6)]. Figs. 9 and 10 exhibit the variation of T_{fi} with respect to the longitudinal ribbon length and temperature, respectively. It appears that in both cases, T_{fi} decreases. However, the rate of the decaying of T_{fi} is higher for $E_0 = 10^6$ V/m than for $E_0 = 10^5$ V/m.

It may be noted from (6) that for a highly asymmetric case, the minimum electron energy is given by $E = \gamma/2\sqrt{2}$. However, for a simplified analytical formulation, we have considered $E \geq \sqrt{2}\gamma$ by taking $n_{1\text{-D}} = 10^9$ m^{-1} for consistency with the Fermi energy. We also note that for degenerate highly asymmetric BGN, the maximum longitudinal bias that can be applied suffers the inequality $v_D(x) \leq (1/e)\left(E_F - \sqrt{2}\gamma\right)$ for each different subband level.

In reality, G_{fi} depends on the collective scattering mechanism suffered during the transport process. The numerical value of G_{fi} near the Fermi energy at lower temperatures may become extremely high even for a very low electric field and in the presence of other scattering mechanisms. We have not extended the appropriate plots below the ballistic length, since in that case, $\lambda_{fi} > L$ and G_{fi} become independent of L. A similar case for a parabolic potential profile between source and drain could have been done as in [20] for 1-D material, which follows parabolic energy dispersion relations. In such a case, only the expression $\xi_{\pm}(\epsilon, n_y)$ in (13) would be modified.

We wish to state that the results obtained in this paper may find important applications in defining the diffusive current transport in BGN FETs. On replacing the electron energy as Fermi energy in (15), the transmission coefficient can readily be calculated to produce the basic current–voltage relationship in BG transistors [24]. However, for an asymmetric BG with very short ribbon width for, e.g., 1–5 nm, it is expected that a negative differential conductivity will exhibit due to the population inversion in the subbands as stated in this paper. This is not particularly featured in BG-based FETs [25] since with the increase in the asymmetry, near $k_x = 0$ region, the bulging of the lower conduction band occurs. This increases the bandgap instead of decreasing, and hence, no population inversion occurs.

A direct application of our simplified result lies in the determination of the other diffusive transport properties like mobility, diffusion constant, Seebeck coefficient, etc., for the analysis of signal transmission under the application of a time-dependent electric field. With the time-dependent drifted occupation probability, it would be of interest to examine the variation of such quantities for the present system. We wish to note that we have not considered the optical and zone boundary phonon scattering mechanisms due to the weak couplings with other graphene lattice phonon modes [9] in this simplified theoretical formalism. The inclusion of the said effects would certainly increase the accuracy of the results, although the qualitative features of the transmission coefficient in degenerate highly asymmetric BGN would not change in the presence of the aforementioned effects. The simplified theory for the diffusive reflection coefficient, as presented in this paper, may find application in transferred electron devices, where resistances can be controlled by opening the gap. The theory developed in this work can also be used to investigate the variation of the effective electron mass, nonlinear response of the carriers, etc., under the influence of external photon fields.

IV. Conclusion

In this paper, we have presented an analytical solution of the carrier reflection coefficient in a twofold degenerate asymmetric BGN under the application of a low static field. For a highly asymmetric ($\triangle = \gamma$) BGN, the density of states in the lower subband increases more than in the upper. Under the LA phonon scattering regime, the formation of two distinct sets of energy subbands signatures a quantized transmission coefficient

as a function of ribbon width and length. The splitting of both conduction bands results an extremely high value of Landauer conductance even at room temperature. The transmission coefficient becomes a quantized function of ribbon width. About 92%–65% of carriers gets transferred from source to drain for a ribbon width of 1–7 nm at room temperature. The well-known result for ballistic conditions has been obtained as a special case of the present analysis under certain limiting conditions and forms an indirect test of our theoretical formalism.

APPENDIX

Modeling the BG as a two coupled hexagonal lattice with a stacking pair of A'–B type, the use of (1) and a Bloch-type eigenstates $\Psi(x,y) = (\psi_A, \psi_{B'}, \psi_{A'}, \psi_A)$, where $\psi_i(x,y) = \phi_i(y)\, e^{ik_x x}$, in which, $i = A, B, A', B'$, leads to the following equations:

$$-v_F\hbar\left(\frac{\partial}{\partial y} - k_x\right)\phi_B = \left(E + \frac{\triangle}{2}\right)\phi_A \tag{17}$$

$$v_F\hbar\left(\frac{\partial}{\partial y} + k_x\right)\phi_{A'} = \left(E - \frac{\triangle}{2}\right)\phi_{B'} \tag{18}$$

$$-v_F\hbar\left(\frac{\partial}{\partial y} - k_x\right)\phi_{B'} = \left(E - \frac{\triangle}{2}\right)\phi_{A'} - \gamma\phi_B \tag{19}$$

$$v_F\hbar\left(\frac{\partial}{\partial y} + k_x\right)\phi_A = \left(E + \frac{\triangle}{2}\right)\phi_B - \gamma\phi_{A'}. \tag{20}$$

Taking the values of $\phi_{B'}$ and ϕ_A from (18) and (17) and substituting them in (19) and (20), respectively, results in

$$\left[\left(k_x^2 - \frac{\partial^2}{\partial y^2}\right) - \left(\frac{E - \triangle/2}{v_F\hbar}\right)^2\right]\phi_{A'} + \gamma\frac{E - \triangle/2}{(v_F\hbar)^2}\phi_B = 0 \tag{21}$$

and

$$\gamma\frac{E + \triangle/2}{(v_F\hbar)^2}\phi_{A'} + \left[\left(k_x^2 - \frac{\partial^2}{\partial y^2}\right) - \left(\frac{E + \triangle/2}{v_F\hbar}\right)^2\right]\phi_B = 0. \tag{22}$$

Assuming the potentials to be constants, the solution is given by

$$\left\{k^2 - \left(\frac{E - \triangle/2}{v_F\hbar}\right)^2\right\}\left\{k^2 - \left(\frac{E + \triangle/2}{v_F\hbar}\right)^2\right\} - \gamma^2\left[\frac{E^2 - \triangle^2/4}{(v_F\hbar)^4}\right] = 0 \tag{23}$$

in which $k^2 = k_x^2 + k_y^2$. However, for a symmetric case ($\triangle = \phi_1 - \phi_2 = 0$), (23) results in

$$\left\{k^2 - \left(\frac{E}{v_F\hbar}\right)^2\right\} = \pm\gamma\frac{E}{(v_F\hbar)^2} \tag{24}$$

which at $k = 0$ simplifies as either $E = 0$ or $E = \pm\gamma$ for both $E > 0$ and $E < 0$ energy bands. This convergence is in accordance with the well-known result [23] and proves the mathematical compatibility of our theory.

For asymmetric BGN, we invoke the VHS condition $k_y = n_y\pi/l_y$ for a Bloch-type wavefunction along the y-direction, which result in,

$$\left\{k_x^2 + \left(\frac{n_y\pi}{l_y}\right)^2 - \left(\frac{E - \triangle/2}{v_F\hbar}\right)^2\right\}\left\{k_x^2 + \left(\frac{n_y\pi}{l_y}\right)^2 - \left(\frac{E + \triangle/2}{v_F\hbar}\right)^2\right\} = \gamma^2\left[\frac{E^2 - \triangle^2/4}{(v_F\hbar)^4}\right]. \tag{25}$$

Equation (3) is the direct consequence of (25).

REFERENCES

[1] A. H. C. Neto, F. Guinea, N. M. R. Peres, K. S. Novoselov, and A. K. Geim, "The electronic properties of graphene," *Rev. Mod. Phys.*, vol. 81, pp. 109–162, 2009.

[2] A. Naeemi and J. D. Meindl, "Compact physics-based circuit models for graphene nanoribbon interconnects," *IEEE Trans. Elec. Dev.*, vol. 56, no. 9, pp. 1822–1833, Sep. 2009.

[3] E. V. Castro, K. S. Novoselov, S. V. Morozov, N. M. R. Peres, J. M. B. Lopes, dos Santos, J. Nilsson, F. Guinea, A. K. Geim, and A. H. Castro, "Biased bilayer graphene: Semiconductor with a gap tunable by the electric field effect," *Phys. Rev. Lett.*, vol. 99, pp. 216802–216805, 2007.

[4] T. Ohta, A. Bostwick, T. Seyller, K. Horn, and E. Rotenberg, "Controlling the electronic structure of bilayer graphene," *Science*, vol. 313, pp. 951–954, 2006.

[5] E. McCann, "Asymmetry gap in the electronic band structure of bilayer graphene," *Phys. Rev. B*, vol. 74, pp. 161403-1–161403-4, 2006.

[6] R. Ma, L. J. Zhu, L. Sheng, M. Liu, and D. N. Sheng, "Quantum Hall effect in biased bilayer graphene," *Eur. Phys. Lett.*, vol. 87, pp. 17009-1–17009-5, 2009.

[7] E. McCann and V. I. Falko, "Landau-level degeneracy and quantum hall effect in a graphite bilayer," *Phys. Rev. Lett.*, vol. 96, pp. 086805-1–086805-4, 2006.

[8] E. A. Henriksen, Z. Jiang, L.-C. Tung, M. E. Schwartz, M. Takita, Y.-J. Wang, P. Kim, and H. L. Stormer, "Cyclotron resonance in bilayer graphene," *Phys. Rev. Lett.*, vol. 100, pp. 087403-1–087403-4, 2008.

[9] E. H. Hwang and S. Das Sarma, "Acoustic phonon scattering limited carrier mobility in two-dimensional extrinsic graphene," *Phys. Rev. B*, vol. 77, pp. 115449-1–115449-6, 2008.

[10] S. S. Kubakaddi, "Interaction of massless Dirac electrons with acoustic phonons in graphene at low temperatures," *Phys. Rev. B*, vol. 79, pp. 075417-1–075417-6, 2008.

[11] M. Barbier, P. Vasilopoulos, F. M. Peeters, and J. M. Pereira, Jr., "Bilayer graphene with single and multiple electrostatic barriers: Band structure and transmission," *Phys. Rev. B*, vol. 79, pp. 155402-1–155402-8, 2009.

[12] M. Koshino and T. Ando, "Transport in bilayer graphene: Calculations within a self-consistent Born approximation," *Phys. Rev. B*, vol. 73, pp. 245403-1–245403-8, 2006.

[13] B. Sahu, H. Min, A. H. MacDonald, and S. K. Banerjee, "Energy gaps, magnetism, and electric-field effects in bilayer graphene nanoribbons," *Phys. Rev. B*, vol. 78, pp. 045404-1–045404-8, 2008.

[14] Y. B. Zhang, Y. W. Tan, H. L. Stormer, and P. Kim, "Experimental observation of the quantum Hall effect and Berrys phase in graphene," *Nature*, vol. 438, pp. 201–204, 2005.

[15] C. Berger, Z. Song, T. Li, X. Li, A. Y. Ogbazghi, R. Feng, Z. Dai, A. N. Marchenkov, E. H. Conrad, P. N. First, and W. A. de Heer, "Ultrathin epitaxial graphite: 2D electron gas properties and a route toward graphene-based nanoelectronics," *J. Phys. Chem. B*, vol. 108, pp. 19912–19916, 2004.

[16] B. E. Feldman, J. Martin, and A. Yacoby, "Broken-symmetry states and divergent resistance in suspended bilayer graphene," *Nature Phys. Lett.*, vol. 5, pp. 889–893, 2009.

[17] M. Lundstrom, *Fundamentals of Carrier Transport*. Cambridge, U.K.: Cambridge Univ. Press, 2000.

[18] L. A. Falkovsky, "Symmetry constraints on phonon dispersion in graphene," *Phys. Lett. A*, vol. 372, pp. 5189–5192, 2008.

[19] P. J. Price, "Hot electrons in a GaAs heterolayer at low temperature," *J. Appl. Phys.*, vol. 53, pp. 6863–6866, 1982.

[20] R. Kimand and M. Lundstrom, "Physics of carrier backscattering in one- and two-dimensional nanotransistors," *IEEE Trans. Electron. Dev.*, vol. 56, no. 1, pp. 132–139, Dec. 2009.

[21] J. P. McKelvey, R. L. Longini, and T. P. Brody, "Alternative approach to the solution of added carrier transport problems in semiconductors," *Phys. Rev.*, vol. 123, no. 1, pp. 51–57, 1961.
[22] J. S. Blakemore, *Semiconductors Statistics*. New York: Dover, 1987.
[23] A. Das, B. Chakraborty, S. Piscanec, S. Pisana, A. K. Sood, and A. C. Ferrari, "Phonon renormalization in doped bilayer graphene," *Phys. Rev. B*, vol. 79, pp. 155417-1–155417-7, 2009.
[24] Y. Ouyang, P. Campbell, and J. Guo, "Analysis of ballistic monolayer and bilayer graphene field-effect transistors," *Appl. Phys. Lett.*, vol. 92, pp. 063120-1–063120-3, 2008.
[25] N. Harada, M. Ohfuti, and Y. Awano, "Performance estimation of graphene field-effect transistors using semiclassical Monte Carlo simulation," *Appl. Phys. Exp.*, vol. 1, pp. 024002-1–024002-3, 2008.

Sitangshu Bhattacharya received the Bachelor's and Master's degrees from the University of Calcutta, Kolkata, India, and the Ph.D. degree from Jadavpur University, Kolkata, in physics and electronic science, in 2001, 2003, and 2009.

He is currently a Postdoctoral Young Scientist at the Centre for Electronics Design and Technology, Indian Institute of Science, Bangalore, India. His current research interests include the theoretical investigation of different diffusive mode electronic and transport properties of low-dimensional structures and devices under external controlled fields using tight binding theory. He has coauthored three monographs entitled *Einstein Relation in Compound Semiconductors and Their Nanostructures*, *Photoemission from Optoelectronic Materials and their Nanostructures* and *Thermoelectric Power in Nanostructured Materials Under Strong Magnetic Field* in the Springer Series in Materials Science and Nanostructured Science and Technology. Besides, he is also the author or coauthor of more than 35 journal publications.

Dr. Bhattacharya was also an Invited Speaker at the XXIXth International Union of Radio Science (URSI, Head Quarters at Belgium), under the International Council of Science (ICSU), General Assembly (GA) held at the University of Chicago.

Santanu Mahapatra (M'08) received the B.E. degree in electronics and telecommunication from Jadavpur University, Kolkata, India, in 1999, the M.Tech. degree in electrical engineering with specialization in microelectronics from the Indian Institute of Technology (IIT), Kanpur, India, in 2001, and the Ph.D. degree in electrical engineering, from the Swiss Federal Institute of Technology Lausanne (EPFL), Lausanne, Switzerland, in 2005.

Since 2005, he has been an Assistant Professor at the Centre for Electronics Design and Technology (CEDT), Indian Institute of Science (IISc), Bangalore, India. He is the Founder of the Nano Scale Device Research Laboratory, CEDT, during 2006, where his team was engaged in research on compact modeling and simulation of emerging nanotechnologies and advanced CMOS devices. He has supervised several doctoral and master thesis. He is the author or coauthor of several papers published in international journals and refereed conferences. He is also the author of the book *Hybrid CMOS Single Electron Transistor Device and Circuit Design* (Artech House, 2006). His current research interests include device reliability, multigate transistors, tunnel FETs, single-electron transistors, and CMOS-nano hybridization.

Dr. Mahapatra received the Best Paper Award in the International Semiconductor Conference (CAS), Romania, in 2003. He is also the recipient of IBM Faculty Award in 2007, Microsoft India Research Outstanding Faculty Award, in 2007, and the associateship of the Indian Academy of Science in 2009.